Received: 13 September 2023 | Revised: 6 April 2024 | Accepted: 10 April 2024

DOI: 10.1002/JPER.23-0370

JOURNAL OF Periodontology

ORIGINAL ARTICLE

Ultrasound-based jawbone surface quality evaluation after alveolar ridge preservation

Amanda B. Rodriguez[1] | **Oliver D. Kripfgans**[2] | **Kenneth M. Kozloff**[3,4] | **Ankita Samal**[2] | **Jae-man Woo**[2] | **Mostafa Shehabeldin**[1] | **Hsun-Liang Chan**[1]

[1]Department of Periodontics and Oral Medicine, School of Dentistry, University of Michigan, Ann Arbor, Michigan, USA

[2]Department of Radiology, Michigan Medicine, University of Michigan, Ann Arbor, Michigan, USA

[3]Department of Biomedical Engineering, University of Michigan Medical School, Ann Arbor, Michigan, USA

[4]Department of Orthopedic Surgery, University of Michigan Medical School, Ann Arbor, Michigan, USA

Correspondence
Oliver D. Kripfgans, Department of Radiology, University of Michigan, 6410B Med Sci I, 1301 Catherine Street, Ann Arbor, MI 48109-2026, USA.
Email: greentom@umich.edu

Funding information
NIH/NIDCR, Grant/Award Number: 1-R56-DE-030872-01; NIH/NCRR, Grant/Award Number: S10RR026475-01

Abstract

Background: Bone readiness for implant placement is typically evaluated by bone quality/density on 2-dimensional radiographs and cone beam computed tomography at an arbitrary time between 3 and 6 months after tooth extraction and alveolar ridge preservation (ARP). The aim of this study is to investigate if high-frequency ultrasound (US) can classify bone readiness in humans, using micro-CT as a reference standard to obtain bone mineral density (BMD) and bone volume fraction (BVTV) of healed sockets receiving ARP in humans.

Methods: A total of 27 bone cores were harvested during the implant surgery from 24 patients who received prior extraction with ARP. US images were taken immediately before the implant surgery at a site co-registered with the tissue biopsy collection location, made possible with a specially designed guide, and then classified into 3 tiers using B-mode image criteria (1) favorable, (2) questionable, and (3) unfavorable. Bone mineral density (hydroxyapatite) and BVTV were obtained from micro-CT as the gold standard.

Results: Hydroxyapatite and BVTV were evaluated within the projected US slice plane and thresholded to favorable (>2200 mg/cm^3; >0.45 mm^3/mm^3), questionable (1500–2200 mg/cm^3; 0.4–0.45 mm^3/mm^3), and unfavorable (<1500 mg/cm^3; <0.4 mm^3/mm^3). The present US B-mode classification inversely scales with BMD. Regression analysis showed a significant relation between US classification and BMD as well as BVTV. T-test analysis demonstrated a significant correlation between US reader scores and the gold standard. When comparing Tier 1 with the combination of Tier 2 and 3, US achieved a significant group differentiation relative to mean BMD ($p = 0.004$, true positive 66.7%, false positive 0%, true negative 100%, false negative 33.3%, specificity 100%, sensitivity 66.7%, receiver operating characteristics area under the curve 0.86). Similar results were found between US-derived tiers and BVTV.

This is an open access article under the terms of the Creative Commons Attribution-NonCommercial-NoDerivs License, which permits use and distribution in any medium, provided the original work is properly cited, the use is non-commercial and no modifications or adaptations are made.
© 2024 The Authors. *Journal of Periodontology* published by Wiley Periodicals LLC on behalf of American Academy of Periodontology.

JOURNAL OF Periodontology

Conclusion: Preliminary data suggest US could classify jawbone surface quality that correlates with BMD/BVTV and serve as the basis for future development of US-based socket healing evaluation after ARP.

KEYWORDS
alveolar ridge preservation, bone mineral density, bone regeneration, jaw, edentulous, ultrasonography, wound healing

1 | INTRODUCTION

After tooth extraction, a cascade of cellular healing events results in vertical and horizontal bone resorption.[1–4] The extent and magnitude of dimensional changes is dependent on systemic factors,[4,5] such as smoking, and local site characteristics, such as facial wall thickness and the remaining alveolar walls.[6,7] Alveolar ridge preservation (ARP) is a surgical procedure, commonly using bone substitutes to fill the extraction socket in order to reduce bone dimensional alterations.[6–8] Current noninvasive imaging modalities evaluating ridge width and height include 2-dimensional (2D) x-ray, and cone beam computed tomography (CBCT). Invasive methods are ridge mapping and surgical verification.[9–12] Although ARP is widely indicated in dental practice for its effectiveness in preserving ridge dimensions,[3,5–8,13–16] evidence also shows that it changes bone density.[1,4–8,11,13–20] Bone density is another important parameter for implant function and longevity.[1,2,5,6,8,11,13–15,17,19–28] Additionally, a standard healing time of 3–6 months has been recommended.[5,7,8,16,29] Postsurgical complications may arise from persistent inflammation, infection, loss of bone grafts, and negative soft- and hard-tissue changes.[2,3,7,14–16] It is not uncommon, that failed ARP may only be found at the time of implant placement, requiring an additional bone grafting procedure or a surgical modification, and having a higher risk for implant complications.[30] Early diagnosis of unfavorable socket healing could potentially allow for early intervention and a reduction in treatment time. A customized time schedule tailored to each surgical site is desirable and yet to be established.

Medical CT can provide Hounsfield Units that correlate with absolute bone density but are not used currently for implant planning due to radiation concerns. Two-D x-rays, projection images, can provide pixel values as a subjective means to evaluate bone density.[11,18,20,23,25,31] CBCT offers valuable insight into bone morphology and dimensions due to its cross-sectional nature; however, its relative voxel values, radiation exposure, low soft tissue contrast, and image artifacts from proximal radio-dense (metallic) objects are among the disadvantages.[24,32–34] In a research setting, quantitative analysis with micro-CT is currently the gold standard to evaluate bone mineral density (BMD) in units of hydroxyapatite (HA) in mg to cubic cm,[6,21–23,35] and bone volume fraction (BVTV) in units of mm^3/mm^3.[36–38] BMD has a highly significant correlation with implant insertion torque.[18,19,25,27,39] BVTV is the volume of mineralized bone per unit volume of the sample and has been shown to serve as an objective indicator for BMD in the implant site and correlated with implant's initial stability.[40]

Ultrasound (US) as a nonionizing, noninvasive, real-time, and chairside modality can image soft- and hard-tissue surfaces on a cross-sectional view plane and would be a desirable tool to evaluate healing longitudinally.[9,32,33,41–47] Thanks to recent improvements in probe miniaturization and higher spatial resolution, US has been successfully used to assess crestal bone surface quality, soft-tissue dimensions, and tissue quality in the oral cavity.[45,46,48,49] US has shown a 91% agreement with CBCT when comparing the cortical bone thickness of edentulous ridges.[24] Furthermore, previous studies validated the feasibility of high-resolution US to estimate edentulous crestal ridge width.[43,45,46] In light of the limitations of the current clinically available radiographic imaging modalities, this preliminary study aims to investigate if high-frequency, point-of-care US can differentiate micro-CT-derived bone density of healed sockets receiving ARP in humans.

2 | MATERIALS AND METHODS

2.1 | Study design and subject recruitment

The present study was approved by the University of Michigan Medical School Institutional Review Board (IRB) (HUM00203875), in accordance with the Helsinki Declaration of 1975, as revised in 2013. Informed consent was obtained from all individuals who participated in the study. The design is a single-blinded, dual comparative study of US with micro-CT in 1 study group.

2.2 | Setting and participants

Subjects, who had already received extraction with ARP and had been scheduled for dental implant surgery, were recruited between January 2022 and December 2022. The inclusion criteria were: (1) age of 18 years or older at enrollment, (2) any edentulous site that received ARP as a standard clinical procedure for at least 4 months, and (3) already scheduled for dental implant surgery according to standard-of-care treatment. Exclusion criteria included: (1) no baseline or incomplete clinical data and (2) tissue core biopsy could not be performed or analyzed. The patient recruitment process, clinical assessment, ultrasonographic examination, and tissue core biopsy were performed by 2 calibrated study members (H.L.C. and A.B.R.). Calibration was performed using a prototype, full-sized, 3D, periodontal US phantom created by our group in collaboration with CIRS Inc. (PIRATE, Model 134200, CIRS Inc., Virginia, USA). Seven data pairs compared guided and freehand images for the phantom's edentulous ridge. The data were analyzed for repeatability by computing the mean (μ) and standard deviation (σ) of the guided and nonguided (freehand) values. Soft- and hard-tissue distances from the reference standard were computed for repeatability, with guided scans having 2.2 times less standard deviation for soft tissue and 1.6 times less for bone. The coefficient of variation remained similar at 22.3% and 26.8% for soft tissue and 50.7% and 42.4% for bone in guided and nonguided scans, respectively.

2.3 | Ultrasonographic image acquisition

The grafted sites were US imaged immediately before the implant surgery, using a commercially available linear array (64-μm axial image resolution) and miniature-sized (≈30-mm long × 18-mm wide × 12-mm thick) probe[*]. Second harmonic imaging (12–24 MHz) and spatial compounding (3 angles) were used for achieving optimal delineation of the soft- and hard-tissues in the virtual convex field of view (~14 mm wide, 15 mm deep). Brightness mode (B-mode) images were obtained by placing the transducer into a 3D registered reference guide based on the intraoral optical and CBCT scan previously taken (A.B.R.) (Figure 1). Anatomical data from CBCT and intraoral optical scans of the edentulous sites were saved in "Digital Imaging and Communication in Medicine" (DICOM) format and the "Standard Tessellation Language" (STL) format, respectively. The US guide creation followed a digital workflow: image acquisition, computer-aided-design (CAD), and computer-aided-manufacturing (CAM). Implant planning was determined based on available soft- and hard-tissue surfaces and clinical criteria. The US guide was designed using the CAD file of the transducer housing in 3 planes: axial, coronal, and sagittal. The US housing was oriented in 3D space (translational and rotational) for imaging the site of implant placement. In other words, the virtual implant abutment was centered within the aperture. In the axial plane, the probe was angled to ensure the image ran parallel to the implant. A "platform part" was added around the housing for US probe support, and a "splint part" was designed for stability with adjacent teeth (Figure 1A, C). Additionally, the planned implant and respective abutment served as references for the bone core biopsy guide design (Figure 1B, D). Therefore, the US images were taken at the same location where the bone core biopsy was harvested during the implant surgery.

2.4 | Tissue biopsy collection and sample preparation

A 3D-printed guide with the desired implant position that was co-registered with the image location was used to obtain the bone core. A 2.8 mm internal diameter trephine drill was used to collect approximately 4 mm (length) bone core and placed in 10% formalin for 24 h and then moved to 70% ethyl alcohol. To maintain tissue orientation a radiopaque gutta-percha cone was placed in the mesial aspect of the core, in a coronal orientation. Special care was taken to use a small size cone at a relative distance from the sample to avoid an artifact image on the sample.

2.5 | Micro-CT samples

The tissue biopsies were placed in a 14 mm diameter specimen holder and scanned using a micro-CT system[†]. Scan settings were voxel size 5 μm, 70 kVp, 114 μA, 0.5 mm AL filter, 1000 projections around 180°, and integration time 500 ms. Micro-CT analysis was calibrated in units of absolute HA mg per cm^3, and BVTV in units of mm^3/mm^3. BMD and BVTV values were calculated using a "bone texture" plugin with public domain software (3D Slicer). Bone cores were analyzed individually to create crestal bone surface and intra-alveolar segments. A segmentation of tissue biopsies (cuboid) was created to obtain an absolute BMD in the cortical slice, seen by US. Segmentations were matched to the US slice thickness (500 μm). HA was evaluated within the projected US slice plane (Figure 2).

[*] L30-8, Mindray/Zonare of North America, San Jose, CA, USA.

[†] μCT100 Scanco Medical, Bassersdorf, Switzerland.

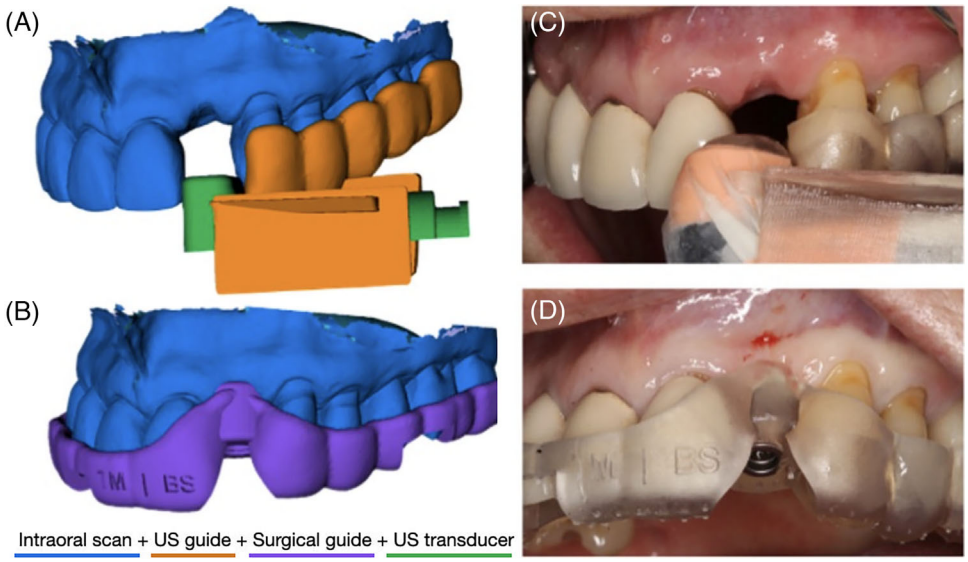


FIGURE 1 (A) 3D depiction of digitally designed and tooth-supported US guide (orange). An intraoral scan of soft and hard tissues is shown in blue. The US transducer (green) is placed, buccal-lingual, to coincide with the location of the tissue biopsy. (B) 3D depiction of a traditional digitally designed surgical guide to obtaining the tissue biopsy and placing the implant. (C) Intraoral photo of a digitally designed and tooth-supported US guide and the US transducer with the probe cover for infection control. (D) Intraoral photo of a digitally designed surgical guide.

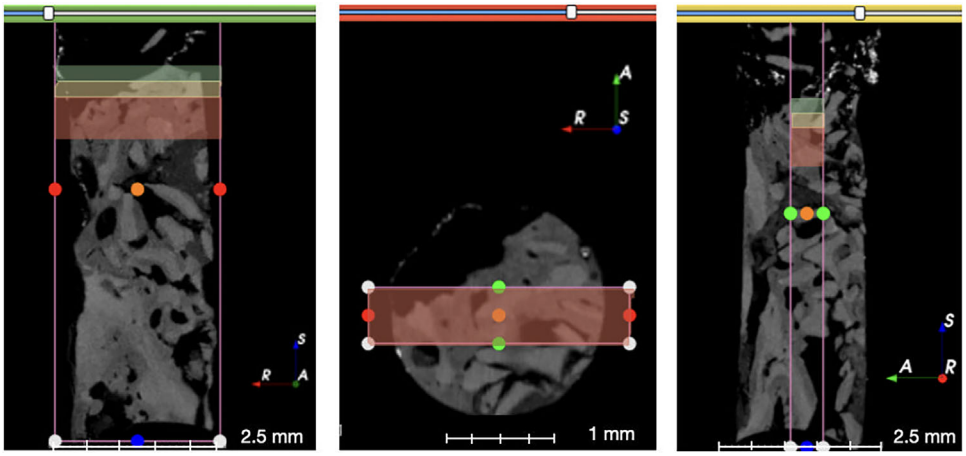


FIGURE 2 Example of a bone core micro-CT image. Segmentation of tissue biopsies (cuboid) to obtain absolute bone mineral density in the cortical slice, seen by US. Segmentations were matched to the US slice thickness (500 μm).

2.6 | US reader score classification

The interface quality between the soft- and hard-tissues was classified by 3 experienced and masked readers (H.L.C., A.B.R., J.W.). A total of 27 US images were each scored by 3 readers at 3 different time points to allow for memory washout, and the mean scores were used for analysis. US images were classified into 1 of 3 classes: favorable (1), questionable (2), and unfavorable (3). This classification was modified from Sinjab et al. 2022[45] (Figure 3).

- Hard-tissue evaluation:
  - Tier 1: A clear, bright/hyperechoic, continuous, and thin interface, indicating the formation of an intact crestal bone surface.
  - Tier 2: Interrupted, less bright/less hyperechoic, irregular, and thicker interface, indicating partial formation of the crestal bone surface.
  - Tier 3: Unclear, interrupted dark/least hyperechoic, irregular, and thick interface, indicating disruption of the crestal bone formation and soft tissue invagination.

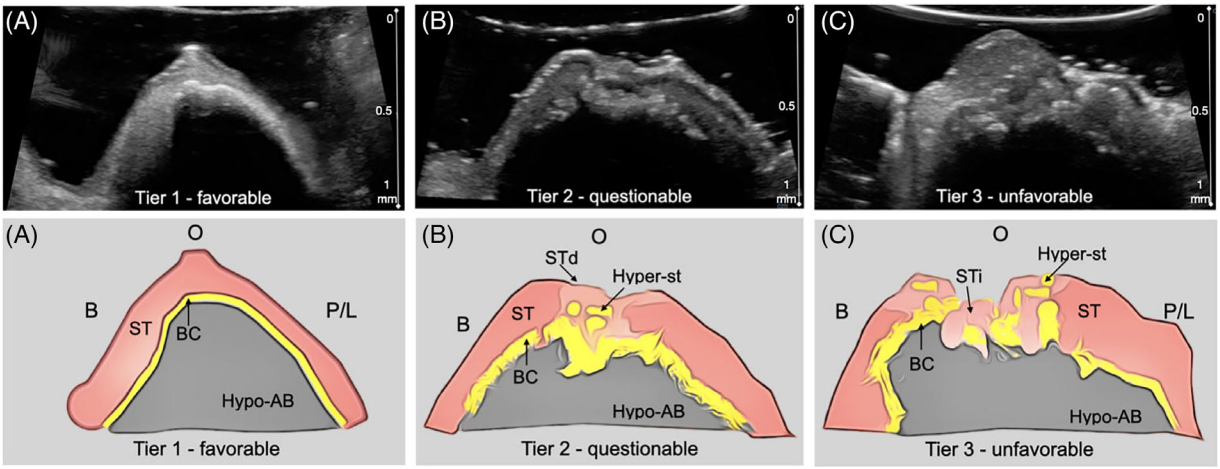


FIGURE 3 Cross-sectional US image examples of the edentulous ridge for 3 distinct cases (top row). (A) Tier 1, favorable healing shows a smooth and homo-echogenic soft tissue layer. The bone crest is a clearly delineated continuous, homogeneous bone surface, and thin interface thus suggesting the formation of an intact crestal bone surface. (B) Tier 2, questionable healing shows soft tissue depression, irregularity, and the presence of hyperechoic structures in the inner submucosal layer. The bone surface is mostly continuous but heterogeneous, indicating the partial formation of crestal bone surface. (C) Tier 3, unfavorable healing shows soft tissue invagination with irregular layers and the presence of hyperechoic structures embedded in the soft tissue. Bone crest has a discontinuous, heterogeneous, irregular, depressed, and thicker interface with the presence of soft tissue invaginations suggesting subpar crestal bone formation. Illustration of the anatomical landmarks in an US B-mode image of an edentulous ridge occlusal view (bottom row). Annotations across the illustrations indicate buccal (B), palatal/lingual (P/L), occlusal (O), soft tissue (ST), bone crest (BC), hypoechoic alveolar bone (Hypo-AB) image below the bone crest, soft tissue depression (STd), hyperechoic structures (Hyperst), soft tissue invagination (STi). (A) Tier 1, (B) Tier 2, (C) Tier 3.

- Soft-tissue evaluation:
  - Tier 1: Smooth epithelial surface with bright/hyperechoic line and a subepithelial hypoechoic layer. The submucosal layer is homo-echogenic. No hyperechoic structures, for example, gas bubbles or bone particle present within the tissues.
  - Tier 2: Depressed epithelial surface with bright/hyperechoic line and a subepithelial hypoechoic layer. Presence of hyperechoic structures, for example, gas bubbles or bone particles present within the tissues.
  - Tier 3: Marked surface depression without clear bright/hyperechoic line and a subepithelial hypoechoic layer. Presence of hyperechoic structures, for example, gas bubbles or bone particles penetrating the full thickness of the tissue layer.

2.7 | Statistical analysis

The micro-CT-derived BMD was compared among the 3 tiers with analysis of variance (ANOVA). The significance level was set at 0.05. All statistical analyses and processing were performed using custom Matlab scripts including its statistics toolbox and commercially available software[‡]. Inter- and intra-reader calibration for US reader scores was performed using intraclass correlation coefficient (ICC). A receiver operating characteristics (ROC) curve was utilized based on the sensitivity and specificity to determine the accuracy of this diagnostic test in identifying favorable and unfavorable healing defined by BMD.

3 | RESULTS

A total of 27 bone cores were harvested from 24 patients (aged 18–90 y/o, median 61, 13 males and 11 females). A total of 11, 7, 4, 4, and 1 sample were from maxillary incisors, maxillary premolars, mandibular incisors, mandibular premolars, and a mandibular molar, respectively. The biomaterials used were mineralized cancellous bone allograft from 2 brands[§,‖] in 15 and 2 sites, respectively, and cortical cancellous mix 50/50 bone allograft[¶] in 10 sites. In addition, absorbable collagen wound dressing [#] in 13 sites, and absorbable collagen membranes from brands [**,††] in 2 and 13 sites, respectively, were used. The median healing period between the extraction surgery plus ARP and the implant surgery when the bone core was

[‡] Prism GraphPad, San Diego, CA, USA.

[§] Puros, ZimVie, Palm Beach Gardens, FL, USA.
[‖] OraGraft, LifeNet Health, Virginia Beach, VA, USA.
[¶] Straumann, Andover, MA, USA.
[#] CollaPlug and CollaTape, ZimVie, Palm Beach Gardens, FL, USA.
[**] BioMend Extend, Zimmer, Palm Beach Gardens, FL, USA.
[††] OraMEM, Salvin Dental, Charlotte, NC, USA.

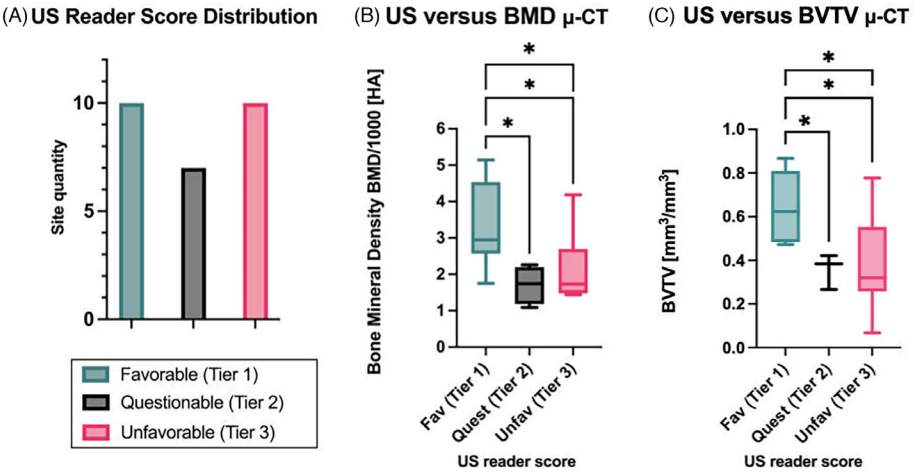


FIGURE 4 (A) US reader score distribution. (B) US tier classification versus BMD micro-CT values. (C) US tier classification versus BVTV micro-CT values.

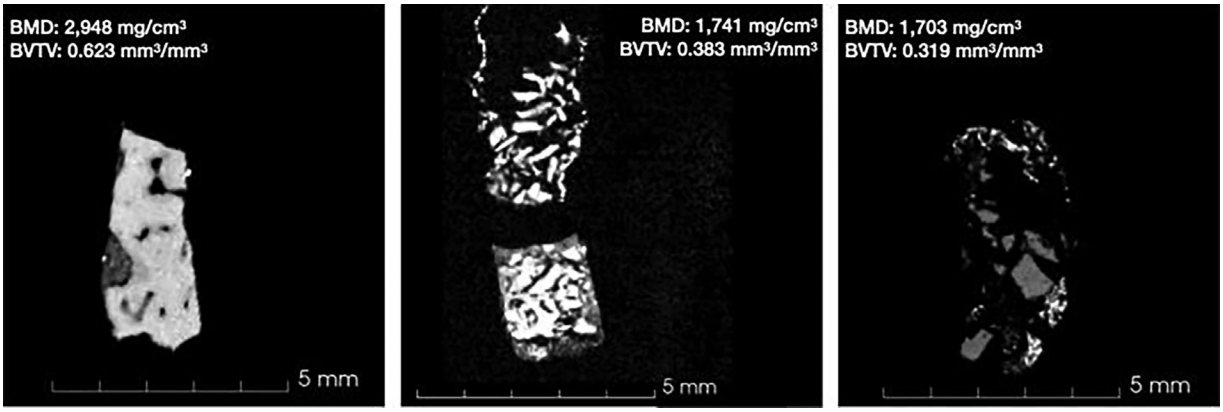


FIGURE 5 Example tissue biopsies with median crestal BMD values and BVTV above, at, and below the threshold were considered favorable, that is, BMD 2200 mg/cm^3 and BVTV 0.45 mm^3/mm^3. The obtained values were compared to the reader score of the US base ridge classification.

collected was 4.4 months ± 12 months (standard deviation) ranging between 3.4 months and 5 years. The reader score classification grouped 10 sites as Tier 1 (favorable), 7 sites as Tier 2 (questionable), and 10 sites as Tier 3 (unfavorable) sites (Figure 4A). The mean ICC intra-reader performance for the 3 time points was 0.923, 0.976, and 0.956 for readers 1, 2, and 3, respectively. Whereas the mean ICC inter-reader performance was 0.877, 0.859, and 0.838, for time points 1, 2, and 3, respectively. The average intra-reader and inter-reader performance was 0.9501 and 0.8315, showing a good to excellent agreement in both cases.[50,51] The median crestal BMD values for Tier 1 were 2948 mg/cm^3, Tier 2 was 1741 mg/cm^3, and Tier 3 with 1703 mg/cm^3 (Figure 5). The mean BVTV values for Tier 1 were 0.623 mm^3/mm^3, Tier 2 was 0.383 mm^3/mm^3, and Tier 3 with 0.319 mm^3/mm^3. T-test analysis demonstrated a significant correlation between US reader scores and the gold standard. For BMD, there was significant difference between Tier 1 versus Tier 2 ($p = 0.020$), between Tier 1 versus Tier 3 ($p = 0.009$) (Figure 4B). The median BMD was significantly higher in Tier 1 versus Tier 2+3 ($p = 0.001$). Similar results were found BVTV values with significant differences between Tier 1 versus Tier 3 ($p = 0.018$), and in Tier 1 versus Tier 2+3 ($p = 0.003$) (Figure 4C).

Samples with a BMD and BVTV value exceeding a threshold of >2200 mg/cm^3 and >0.45 mm^3/mm^3, respectively, were deemed clinically acceptable bone density for implant insertion surgery.[18,21,22,25,52] Furthermore, BMD and BVTV values 1500 mg/cm^3 to 2200 mg/cm^3; 0.4–0.45 mm^3/mm^3 were deemed questionable and <1500 mg/cm^3; <0.4 mm^3/mm^3 unfavorable, respectively. Tier 1 did not show any grafts with a mean BMD less than 2200, thus reflecting a specificity of 100% (Figure 6A, B). Yet, the combination of Tiers 2 and 3 led to a sensitivity of 66.7%. When comparing Tier 1 to Tier 3, that is, removing Tier 2, the specificity remains at 100%;

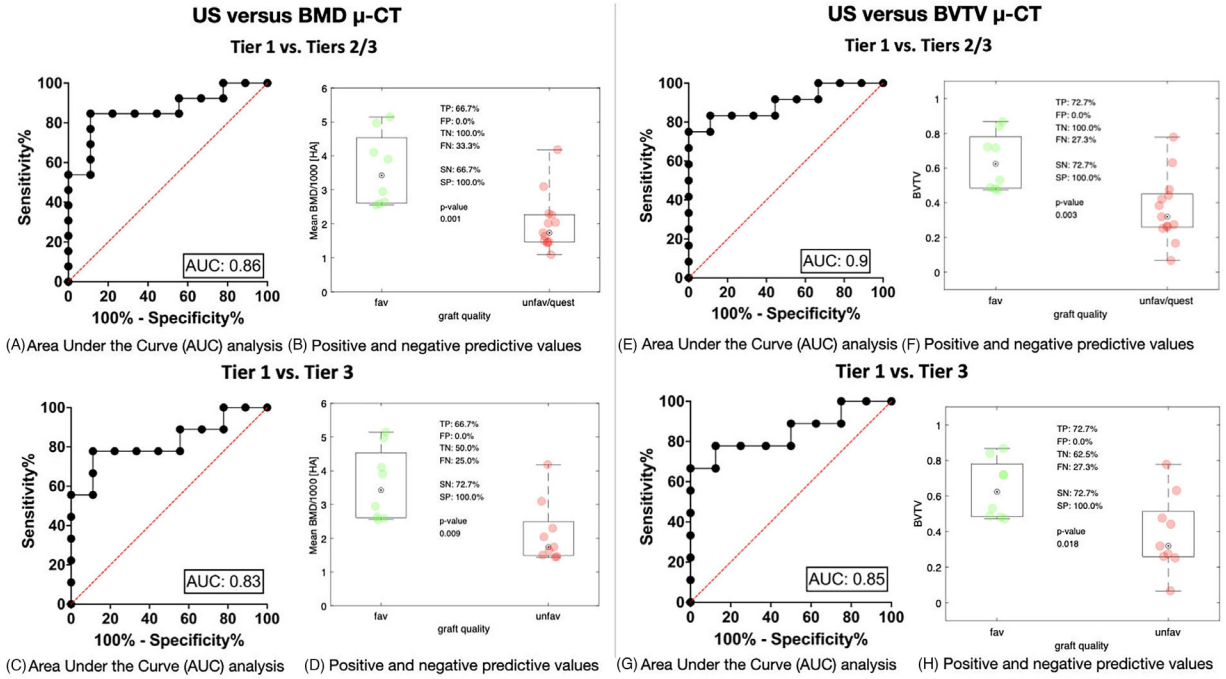


FIGURE 6 (Left panel) Sensitivity and specificity of the US versus BMD test of Tier 1 compared to Tier 2 + 3. (A) AUC showed 0.86 and (B) Positive and negative predictive values between Tier 1 and Tier 2+3 showed specificity (100%), sensitivity (66.7%), and false positive (0%). Sensitivity and specificity of the US test of Tier 1 compared to Tier 3. (C) AUC analysis showed 0.83 and (D) Positive and negative predictive values between Tier 1 and Tier 3 showed specificity (100%), sensitivity (72.7%), and false positives (0%). (Right panel) Sensitivity and specificity of the US versus BVTV test of Tier 1 compared to Tier 2 + 3. (E) AUC showed 0.90 and (F) Positive and negative predictive values between Tier 1 and Tier 2+3 showed specificity (100%), sensitivity (72.7%), and false positive (0%). Sensitivity and specificity of the US test of Tier 1 compared to Tier 3. (G) AUC analysis showed 0.85. (H) Positive and negative predictive values between Tier 1 and Tier 3 showed specificity (100%), sensitivity (72.7%), and false positives (0%).

however, sensitivity increased to 72.7%. The resulting *p*-value increased to 0.009 (Figure 6C, D). In neither scenario are any false positives observed. The area under the curve (AUC) of 0. 86 was obtained when Tier 1 was plotted with Tiers 2+3 (Figure 6A, B), and 0.83 when Tier 1 was plotted with Tier 3 (Figure 6C, D).[53,54] Similar results were found between US-derived Tiers and BVTV. When comparing Tier 1 with the combination of Tier 2 and 3, US achieved a significant group differentiation relative to mean BVTV ($p = 0.003$, true positive 72.7%, false positive 0%, true negative 100%, false negative 27.3%, specificity 100%, sensitivity 72.7%, ROC AUC 0.90 (Figure 6E–H). Regression analysis showed a significant relation between US classification and BMD as well as BVTV (See Supplemental Figure A in online *Journal of Periodontology*).

4 | DISCUSSION

In the present study, the results show that jawbone surface quality classification, based on US, correlates with median BMD and BVTV (p-value < 0.05). AUC values of ~0.9 suggest that US could be able to differentiate cases between BMD > 2200 HA mg per cm^3, BVTV > 0.45 mm^3/mm^3 and those below that threshold. The high specificity (100%) suggested that all cases that did not have BMD or BVTV below the threshold were not classified as Tier 1. In this regard, US gives the clinician the ability to recognize adequately matured grafts, and potentially reduce waiting time from the standard 3–6 months. On the other hand, the presence of a sensitivity of 72.7% for Tier 1 when compared to Tier 3, and 66.7% for Tier 1 when compared to Tier 2 + 3, may be related to the cases that had BMD higher than the threshold but were classified as unfavorable healing on US. These findings were also confirmed when comparing BVTV values with US reader scores. This might be associated with the US scan angles due to the tight space of the edentulous ridge, which precluded a perpendicular image of the bone surface. In these cases, the operator should try to reposition the transducer to obtain a more perpendicular orientation to the bone to avoid false negative interpretations. In other words, the operator should exhaust the effort to rule out the absence of a sharp bone-soft tissue interface by "looking at" the bone surface at different angles to reduce false negatives.

2D X-rays, CBCT, tactile sensation during osteotomy, and implant insertion torque resistance are among the common methods to assess bone density. [20–22,27,28,52] Tactile sensation and torque resistance test are considered late indicators because they are performed during implant surgery. Radiographs can infer bone density prior to the implant surgery; unfortunately, inherent limitations in image forming mechanisms render them not reliable for providing objective bone density assessment.[20,27] Specifically, 2D radiographs could overestimate the bone density with the presence of thick facial and/or lingual plates because of the superimposition of the 3D anatomy.[4,10,23,31,53] CBCT provides relative bone density values that may not be clinically relevant. Bone density evaluation is particularly unreliable with the presence of heterogeneous structures, such as bone particulates and adjacent metallic structures due to the averaging effect from the tomography based estimation. The clinical gold standard for understanding bone density before implant placement is the analysis of BMD and trabecular microstructure on medical CT.[18,19,23,25,27,39] Its equivalence in the research setting is micro-CT. Implant stability strongly depends on quality and quantity of the surrounding bone.[20,55,56] Thus, BMD and BVTV values have been used to assess implant stability preoperatively and have a highly significant correlation with insertion torque.[18,20,25,27,40] Misch and Judy 1987[28] classified bone density into 4 types (D1-D4), from dense cortical bone to fine trabecular bone based on medical CT. Medical CT incurs high radiation dose and is not recommended to be applied repeatedly on the same patients. Consequently, the correlation of BMD with B-mode ultrasonography could potentially bridge this diagnostic gap by serving as a noninvasive qualitative imaging technique for evaluating bone maturation and implant readiness.

The diagnostic value of US in evaluating surface bone density relies on the appearance of the soft-tissue and the hard-soft tissue interface. At a histological level, "a hard tissue bridge-cortical bone-formed, which closed the socket" during normal healing.[2,4,6,8,13–15,48] Progenitor cells originating from the surrounding bone walls migrate centrally to form woven bone that later matures and finishes lastly at the coronal aspect of the socket. Therefore, evaluating surface bone quality could indicate the overall socket healing. A high-intensity (hyperechoic) line in a US image indicates a strong likelihood of the presence of a boundary between the hard- and soft-tissue.[57,58] This high-intensity interface is followed by a low-intensity (hypoechoic) region. This "shadow region" denotes that interior bone surfaces cannot be imaged with US.[26,57–59] In cases of suboptimal healing, various degrees of soft tissue invagination result in the irregularity of this interface and reduced intensity.[45] Sound can penetrate deeper into the healed socket before it bounces back, giving a thicker interface appearance. In totally failed sockets, due to complete soft tissue invagination, the sound can penetrate into the entire socket. In orthopedics, musculoskeletal US has demonstrated clinical values in diagnosing bone fractures and evaluating osteoporosis with a variety of quantitative parameters.[26,57,59–61] These parameters could be applied for evaluating jawbone quality in the future.

Limitations of this study include the small sample size being a proof-of-principle study, reader-dependent evaluation of the US images, inability of micro-CT and US to differentiate bone particulates from new bone, and the angle-dependent imaging acquisition that tends to underestimate the surface bone quality. Future research should focus on the development of a standard scanning protocol, refine the US classification system, and the algorithm-based quantitative bone maturation analysis, including artificial intelligence to reduce reader bias with a larger subject pool.

5 | CONCLUSIONS

Preliminary encouraging data suggested the potential value of US as a noninvasive tool to evaluate bone surface and soft tissue characteristics that correlate with bone mineral density and BVTV.

AUTHOR CONTRIBUTIONS

Amanda B. Rodriguez, Oliver D. Kripfgans, Kenneth M. Kozloff, Ankita Samal, Mostafa Shehabeldin, and Hsun-Liang Chan have made substantial contributions to conception and design of the study. Amanda B. Rodriguez, Oliver D. Kripfgans, Kenneth M. Kozloff, Ankita Samal, Jae-man Woo, Mostafa Shehabeldin, and Hsun-Liang Chan have been involved in data collection and data analysis. Amanda B. Rodriguez, Oliver D. Kripfgans, Kenneth M. Kozloff, Ankita Samal, Mostafa Shehabeldin, and Hsun-Liang Chan have been involved in data interpretation, drafting the manuscript, and revising it critically and have given final approval of the version to be published.

ACKNOWLEDGMENTS

This study was funded by NIH (1-R56-DE-030872-01). The use of the School of Dentistry micro-CT Core was funded in part by NIH/NCRR S10RR026475-01.

CONFLICT OF INTEREST STATEMENT

The authors declare no conflicts of interest.

ORCID

Amanda B. Rodriguez https://orcid.org/0000-0001-6011-6708

Hsun-Liang Chan https://orcid.org/0000-0001-5952-0447

REFERENCES

1. Araújo MG, Lindhe J. Ridge alterations following tooth extraction with and without flap elevation: an experimental study in the dog. *Clin Oral Implants Res*. 2009;20:545-549.
2. Cardaropoli G, Araújo M, Lindhe J. Dynamics of bone tissue formation in tooth extraction sites. An experimental study in dogs. *J Clin Periodontol*. 2003;30:809-818.
3. Chan HL, Lin GH, Fu JH, Wang HL. Alterations in bone quality after socket preservation with grafting materials: a systematic review. *Int J Oral Maxillofac Implants*. 2013;28:710-720.
4. Couso-Queiruga E, Stuhr S, Tattan M, Chambrone L, Avila-Ortiz G. Post-extraction dimensional changes: a systematic review and meta-analysis. *J Clin Periodontol*. 2021;48:126-144.
5. Kim JH, Susin C, Min JH, et al. Extraction sockets: erratic healing impeding factors. *J Clin Periodontol*. 2014;41:80-85.
6. Avila-Ortiz G, Chambrone L, Vignoletti F. Effect of alveolar ridge preservation interventions following tooth extraction: a systematic review and meta-analysis. *J Clin Periodontol*. 2019;46(21):195-223.
7. Lim G, Lin GH, Monje A, Chan HL, Wang HL. Wound healing complications following guided bone regeneration for ridge augmentation: a systematic review and meta-analysis. *Int J Oral Maxillofac Implants*. 2018;33:41-50.
8. MacBeth N, Trullenque-Eriksson A, Donos N, Mardas N. Hard and soft tissue changes following alveolar ridge preservation: a systematic review. *Clin Oral Implants Res*. 2017;28:982-1004.
9. Izzetti R, Vitali S, Gabriele M, Caramella D. Feasibility of a combination of intraoral UHFUS and CBCT in the study of peri-implantitis. *Oral Surg Oral Med Oral Pathol Oral Radiol*. 2019;127:e89-e94.
10. Kroll T, May A, Wittekindt C, et al. Cone beam computed tomography (CBCT) sialography–an adjunct to salivary gland ultrasonography in the evaluation of recurrent salivary gland swelling. *Oral Surg Oral Med Oral Pathol Oral Radiol*. 2015;120:771-775.
11. Pauwels R, Jacobs R, Singer SR, Mupparapu M. CBCT-based bone quality assessment: are Hounsfield units applicable? *Dentomaxillofac Radiol*. 2015;44:20140238.
12. Traxler M, Ulm C, Solar P, Lill W. Sonographic measurement versus mapping for determination of residual ridge width. *J Prosthet Dent*. 1992;67:358-361.
13. Araújo MG, Lindhe J. Dimensional ridge alterations following tooth extraction. An experimental study in the dog. *J Clin Periodontol*. 2005;32:212-218.
14. Araújo MG, Silva CO, Misawa M, Sukekava F. Alveolar socket healing: what can we learn? *Periodontol 2000*. 2015;68:122-134.
15. Barootchi S, Wang HL, Ravida A, et al. Ridge preservation techniques to avoid invasive bone reconstruction: a systematic review and meta-analysis: Naples Consensus Report Working Group C. *Int J Oral Implantol (Berl)*. 2019;12:399-416.
16. Garcia J, Dodge A, Luepke P, Wang HL, Kapila Y, Lin GH. Effect of membrane exposure on guided bone regeneration: a systematic review and meta-analysis. *Clin Oral Implants Res*. 2018;29:328-338.
17. Araújo MG, Lindhe J. Ridge preservation with the use of Bio-Oss collagen: a 6-month study in the dog. *Clin Oral Implants Res*. 2009;20:433-440.
18. Homolka P, Beer A, Birkfellner W, et al. Bone mineral density measurement with dental quantitative CT prior to dental implant placement in cadaver mandibles: pilot study. *Radiology*. 2002;224:247-252.
19. Johansson P. Assessment of bone quality from cutting resistance during implant surgery. *Int J Oral Maxillofac Implants*. 1994;9:279-288.
20. Parsa A, Ibrahim N, Hassan B, van der Stelt P, Wismeijer D. Bone quality evaluation at dental implant site using multislice CT, micro-CT, and cone beam CT. *Clin Oral Implants Res*. 2015;26:e1-7.
21. Beer A, Gahleitner A, Holm A, Birkfellner W, Homolka P. Adapted preparation technique for screw-type implants: explorative in vitro pilot study in a porcine bone model. *Clin Oral Implants Res*. 2007;18:103-107.
22. Beer A, Gahleitner A, Holm A, Tschabitscher M, Homolka P. Correlation of insertion torques with bone mineral density from dental quantitative CT in the mandible. *Clin Oral Implants Res*. 2003;14:616-620.
23. Cann CE. Quantitative CT for determination of bone mineral density: a review. *Radiology*. 1988;166:509-522.
24. Degen K, Habor D, Radermacher K, et al. Assessment of cortical bone thickness using ultrasound. *Clin Oral Implants Res*. 2017;28:520-528.
25. Homolka P, Beer A, Birkfellner W, Gahleitner A, Nowotny R, Bergmann H. Local calibrated bone mineral density in the mandible presented using a color coding scheme. *Med Eng Phys*. 2001;23:673-677.
26. Jacobson JA, Middleton WD, Allison SJ, et al. Ultrasonography of superficial soft-tissue masses: society of radiologists in ultrasound consensus conference statement. *Radiology*. 2022;304:18-30.
27. Lee S, Gantes B, Riggs M, Crigger M. Bone density assessments of dental implant sites: 3. Bone quality evaluation during osteotomy and implant placement. *Int J Oral Maxillofac Implants*. 2007;22:208-212.
28. Misch CE, Judy KW. Classification of partially edentulous arches for implant dentistry. *Int J Oral Implantol*. 1987;4:7-13.
29. Bushahri A, Kripfgans OD, George F, Wang IC, Wang HL, Chan HL. Facial mucosal level of single immediately placed implants with either immediate provisionalization or delayed restoration: an intermediate-term study. *J Periodontol*. 2021;92:1213-1221.
30. Velasquez D, Araújo MG, Clem DS, et al. A prospective, randomized, controlled, multicenter evaluation of extraction socket management comparing a wound dressing and a soft tissue substitute. *Int J Periodontics Restorative Dent*. 2022;42:e161-e174.
31. Rodriguez Betancourt A, Samal A, Chan HL, Kripfgans OD. Overview of ultrasound in dentistry for advancing research methodology and patient care quality with emphasis on periodontal/peri-implant applications. *Z Med Phys*. 2023;33:336-386.
32. Chan H-LA, Kripfgans OD. *Dental Ultrasound in Periodontology and Implantology*. Springer; 2020:161-175.
33. Chan HL, Kripfgans OD. Ultrasonography for diagnosis of peri-implant diseases and conditions: a detailed scanning protocol and case demonstration. *Dentomaxillofac Radiol*. 2020;49:20190445.
34. Vanderstuyft T, Tarce M, Sanaan B, Jacobs R, de Faria Vasconcelos K, Quirynen M. Inaccuracy of buccal bone

thickness estimation on cone-beam CT due to implant blooming: an ex-vivo study. *J Clin Periodontol*. 2019;46:1134-1143.
35. Genant HK, Ettinger B, Cann CE, Reiser U, Gordan GS, Kolb FO. Osteoporosis: assessment by quantitative computed tomography. *Orthop Clin North Am*. 1985;16:557-568.
36. Bohner L, Tortamano P, Gremse F, Chilvarquer I, Kleinheinz J, Hanisch M. Assessment of trabecular bone during dental implant planning using cone-beam computed tomography with high-resolution parameters. *Open Dentist J*. 2021;15:57-63.
37. Kazama JJ, Koda R, Yamamoto S, Narita I, Gejyo F, Tokumoto A. Cancellous bone volume is an indicator for trabecular bone connectivity in dialysis patients. *Clin J Am Soc Nephrol*. 2010;5:292-298.
38. Klintström B, Henriksson L, Moreno R, et al. Photon-counting detector CT and energy-integrating detector CT for trabecular bone microstructure analysis of cubic specimens from human radius. *Eur Radiol Exp*. 2022;6:31. doi:10.1186/s41747-022-00286-w
39. Friberg B, Sennerby L, Roos J, Johansson P, Strid CG, Lekholm U. Evaluation of bone density using cutting resistance measurements and microradiography: an in vitro study in pig ribs. *Clin Oral Implants Res*. 1995;6:164-171.
40. Tian T, Liu HH, Zhang ZH, Han Q, Chen J, Lv J. Correlation between bone volume fraction in posterior implant area and initial implant stability. *Oral Surg Oral Med Oral Pathol Oral Radio*. 2022;133:396-401.
41. Chan HL, Sinjab K, Li J, Chen Z, Wang HL, Kripfgans OD. Ultrasonography for noninvasive and real-time evaluation of peri-implant tissue dimensions. *J Clin Periodontol*. 2018;45:986-995.
42. Chan HL, Wang HL, Fowlkes JB, Giannobile WV, Kripfgans OD. Non-ionizing real-time ultrasonography in implant and oral surgery: a feasibility study. *Clin Oral Implants Res*. 2017;28:341-347.
43. Choi M, Culjat MO, Singh RS, White SN. Ultrasound imagery for dental implant diagnosis and treatment planning in a porcine model. *J Prosthet Dent*. 2012;108:344-353.
44. Moore CA, Law JK, Retout M, et al. High-resolution ultrasonography of gingival biomarkers for periodontal diagnosis in healthy and diseased subjects. *Dentomaxillofac Radiol*. 2022;51:20220044.
45. Sinjab K, Kripfgans OD, Ou A, Chan HL. Ultrasonographic evaluation of edentulous crestal bone topography: a proof-of-principle retrospective study. *Oral Surg Oral Med Oral Pathol Oral Radiol*. 2022;133:110-117.
46. Siqueira R, Sinjab K, Pan YC, Soki F, Chan HL, Kripfgans O. Comprehensive peri-implant tissue evaluation with ultrasonography and cone-beam computed tomography: a pilot study. *Clin Oral Implants Res*. 2021;32:777-785.
47. Tattan M, Sinjab K, Lee E, et al. Ultrasonography for chairside evaluation of periodontal structures: a pilot study. *J Periodontol*. 2020;91:890-899.
48. Kämmerer PW, Kumar VV, Brüllmann D, et al. Evaluation of ultrasound transmission velocity and 3-dimensional radiology in different bone types for dental implantology: a comparative ex vivo study. *Oral Surg Oral Med Oral Pathol Oral Radiol*. 2013;116:e77-84.
49. Veltri M, Valenti R, Ceccarelli E, Balleri P, Nuti R, Ferrari M. The speed of sound correlates with implant insertion torque in rabbit bone: an in vitro experiment. *Clin Oral Implants Res*. 2010;21:751-755.
50. Cicchetti DV. Guidelines, criteria, and rules of thumb for evaluating normed and standardized assessment instruments in psychology. *Psychological Assessment*. 1994;6:284.
51. Koo TK, Li MY. A guideline of selecting and reporting intraclass correlation coefficients for reliability research. *J Chiropr Med*. 2016;15:155-163.
52. Nakahara K, Haga-Tsujimura M, Igarashi K, et al. Single-staged implant placement using the bone ring technique with and without membrane placement: micro-CT analysis in a preclinical in vivo study. *Clin Oral Implants Res*. 2020;31:29-36.
53. Maupomé G, Schrader S, Mannan S, Garetto L, Eggertsson H. Diagnostic thinking and information used in clinical decision-making: a qualitative study of expert and student dental clinicians. *BMC Oral Health*. 2010;10:11. doi:10.1186/1472-6831-10-11
54. Mileman PA, van den Hout WB. Evidence-based diagnosis and clinical decision making. *Dentomaxillofac Radiol*. 2009;38:1-10.
55. Lang TF, Augat P, Lane NE, Genant HK. Trochanteric hip fracture: strong association with spinal trabecular bone mineral density measured with quantitative CT. *Radiology*. 1998;209:525-530.
56. Premnath K, Sridevi J, Kalavathy N, Nagaranjani P, Sharmila MR. Evaluation of stress distribution in bone of different densities using different implant designs: a three-dimensional finite element analysis. *J Indian Prosthodont Soc*. 2013;13:555-559.
57. Hacihaliloglu I, Guy P, Hodgson AJ, Abugharbieh R. Automatic extraction of bone surfaces from 3D ultrasound images in orthopaedic trauma cases. *Int J Comput Assist Radiol Surg*. 2015;10:1279-1287.
58. Jain AK, Taylor RH. Understanding bone responses in B-mode ultrasound images and automatic bone surface extraction using a Bayesian probabilistic framework. *Medical imaging2004: ultrasonic imaging and signal processing*. Spie; 2004:131-142.
59. Parmar BJ, Yang X, Chaudhry A, et al. Ultrasound elastography assessment of bone/soft tissue interface. *Phys Med Biol*. 2016;61:131-150.
60. Chan V, Perlas A. Basics of ultrasound imaging. *Atlas of ultrasound-guided procedures in interventional pain management*. 2011:13-19.
61. Hacihaliloglu I. Ultrasound imaging and segmentation of bone surfaces: a review. *Technology (Singap World Sci)*. 2017;5:74-80.

SUPPORTING INFORMATION

Additional supporting information can be found online in the Supporting Information section at the end of this article.

How to cite this article: Rodriguez AB, Kripfgans OD, Kozloff KM, et al. Ultrasound-based jawbone surface quality evaluation after alveolar ridge preservation. *J Periodontol*. 2024;95:1150–1159. https://doi.org/10.1002/JPER.23-0370